

GranuSAS: Software of rapid particle size distribution analysis from small angle scattering data

Qiaoyu Guo(郭桥雨), Fei Xie(谢飞), Xuefei Feng(冯雪飞), Zhe Sun(孙喆), Changda Wang(王昌达), and Xuechen Jiao(焦学琛)

Citation: Chin. Phys. B, 2026, 35 (**2**): 027802. DOI: 10.1088/1674-1056/ae37f4
http://cpb.iphy.ac.cn; http://iopscience.iop.org/cpb

What follows is a list of articles you may be interested in

Preparation and photoelectric properties of cadmium sulfide quantum dots

Yue Gu(古月), Libin Tang(唐利斌), Xiaopeng Guo(郭小鹏), Jinzhong Xiang(项金钟), Kar Seng Teng, Shu Ping Lau(刘树平)

Chin. Phys. B, 2019, 28 (**4**): 047803. DOI: 10.1088/1674-1056/28/4/047803

Restructuring of plasmonic nanoparticle aggregates with arbitrary particle size distribution in pulsed laser fields

A E Ershov, A P Gavrilyuk, S V Karpov, S P Polyutov

Chin. Phys. B, 2016, 25 (**11**): 117806. DOI: 10.1088/1674-1056/25/11/117806

Apparent directional spectral emissivity determination of semitransparent materials

Chun-Yang Niu(牛春洋), Hong Qi(齐宏), Ya-Tao Ren(任亚涛), Li-Ming Ruan(阮立明)

Chin. Phys. B, 2016, 25 (**4**): 047801. DOI: 10.1088/1674-1056/25/4/047801

In-situ SAXS study on PET/ PMMT composites during tensile tests

Wei-Dong Cheng(程伟东), Xiao-Hua Gu(顾晓华), Xue Song(宋雪), Peng Zeng(曾鹏), Zhao-Jun Wu(吴昭君), Xue-Qing Xing(邢雪青), Guang Mo(默广), Zhong-Hua Wu(吴忠华)

Chin. Phys. B, 2016, 25 (**1**): 017802. DOI: 10.1088/1674-1056/25/1/017802

COMPUTATIONAL PROGRAMS FOR PHYSICS

GranuSAS: Software of rapid particle size distribution analysis from small angle scattering data

Qiaoyu Guo(郭桥雨), Fei Xie(谢飞), Xuefei Feng(冯雪飞), Zhe Sun(孙喆), Changda Wang(王昌达)[†], and Xuechen Jiao(焦学琛)[‡]

National Synchrotron Radiation Laboratory, University of Science and Technology of China, Hefei 230029, *China*

(Received 30 September 2025; revised manuscript received 9 January 2026; accepted manuscript online 14 January 2026)

Small angle x-ray scattering (SAXS) is an advanced technique for characterizing the particle size distribution (PSD) of nanoparticles. However, the ill-posed nature of inverse problems in SAXS data analysis often reduces the accuracy of conventional methods. This article proposes a user-friendly software for PSD analysis, GranuSAS, which employs an algorithm that integrates truncated singular value decomposition (TSVD) with the Chahine method. This approach employs TSVD for data preprocessing, generating a set of initial solutions with noise suppression. A high-quality initial solution is subsequently selected via the *L*-curve method. This selected candidate solution is then iteratively refined by the Chahine algorithm, enforcing constraints such as non-negativity and improving physical interpretability. Most importantly, GranuSAS employs a parallel architecture that simultaneously yields inversion results from multiple shape models and, by evaluating the accuracy of each model's reconstructed scattering curve, offers a suggestion for model selection in material systems. To systematically validate the accuracy and efficiency of the software, verification was performed using both simulated and experimental datasets. The results demonstrate that the proposed software delivers both satisfactory accuracy and reliable computational efficiency. It provides an easy-to-use and reliable tool for researchers in materials science, helping them fully exploit the potential of SAXS in nanoparticle characterization.

Keywords: small angle x-ray scattering, data analysis software, particle size distribution, inverse problem

PACS: 78.70.Ck, 88.40.fc, 75.50.Tt, 02.30.Zz

DOI: 10.1088/1674-1056/ae37f4 **CSTR:** 32038.14.CPB.ae37f4

1. Introduction

Particle size distribution (PSD), as an important structural parameter of materials, plays a crucial role in many fields including semiconductors, biology, medicine, and food.[1–3] In materials science, the PSD directly influences their physical and chemical properties.[4–6] For instance, in metal powders, PSD shows impact on its bulk density, flowability, sintering behavior, and the mechanical properties of the final product.[7,8] Proper mixing of fine and coarse particles can increase packing density in metal powders.[9] In pharmaceutical sciences, the PSD of drug particles could affect solubility, dispersibility, and bioavailability, thereby impacting drug efficacy and safety.[10,11] Consequently, accurate PSD characterization is essential for understanding material properties and optimizing material performance.

Small angle x-ray scattering (SAXS) is a practical method for characterizing PSD.[12–14] It measures x-ray scattering images within a small angle range of 0°–5° near the incident beam passing through the sample.[15] For polymer materials, SAXS can measure the size and shape of polymer particles, analyze the phase structure of blended polymers, and determine long-period spacing, branching degree and molecular chain length.[16] Moreover, SAXS is powerful for characterizing pore architectures in nanostructured materials, including their size distribution, morphology, and spatial arrangement.[17,18]

In the computational analysis of PSD, two primary methodological frameworks are commonly employed: model-dependent analytical method and numerical matrix inversion method.[19] The conventional stepwise tangent method is a classic model-dependent approach,[20] which segmentally linearizes the scattering intensity curve and sequentially solves for the distribution characteristics across different size intervals using the Guinier approximation. While computationally efficient for monodisperse systems, this analytical method demonstrates reduced accuracy when applied to polydisperse systems. The numerical matrix inversion method transforms this problem into solving a system of linear equations, essentially addressing a Fredholm integral equation. Truncated singular value decomposition (TSVD) is a commonly used method,[21–23] which improves computational stability by removing noise through matrix decomposition. However, the truncation process can lead to information loss, resulting in non-physical phenomena such as negative values. The Chahine algorithm iteratively refines a pre-set PSD to approx-

[†]Corresponding author. E-mail: wchda@ustc.edu.cn

[‡]Corresponding author. E-mail: xjiao@ustc.edu.cn

© 2026 Chinese Physical Society and IOP Publishing Ltd. All rights, including for text and data mining, AI training, and similar technologies, are reserved.

imate the true distribution from the SAXS data.[24] However, it depends on the accuracy of the initial values, and if the pre-set value is inaccurate, the algorithm may fail to converge. Meanwhile, the Monte Carlo method (for the open source software — McSAS) may solve problems through random simulation,[25,26] but its slow convergence speed (may require minutes or even hours of PSD computation) renders it impractical for time-resolved SAXS experiments. In the maximum entropy method (for the commercial software Igor Pro — Irena), the objective function is the maximization of entropy. In the absence of prior information, this approach preserves as much diversity in the particle-size distribution as possible. However, in many cases, this method may fail to converge upon a solution.

This work proposes a PSD analysis software named GranuSAS, which is based on a TSVD-optimized Chahine algorithm. The TSVD-optimized Chahine algorithm first employs TSVD to generate an initial solution with noise suppression, which is then refined through Chahine's iterative inversion method. Furthermore, the software innovatively incorporates a parallel computing mechanism for multi-shape modeling, which simultaneously outputs results from multiple models and recommends the optimal shape without requiring any prior knowledge. To validate its reliability, several tests were conducted using simulated data of various shapes and dispersity, as well as experimental data from polystyrene nanospheres. In terms of computational efficiency, GranuSAS demonstrates a significant improvement over the McSAS software, and its superior computational speed provides an efficient and reliable new tool for PSD inversion.

2. Methods

2.1. Mathematical physical model

The SAXS data, rich in nanoscale structural information — particularly regarding size distribution — enable the extraction of key parameters such as nanoparticle size, shape, and dispersion state through systematic analysis. To verify the accuracy of the inversion, it is necessary to generate some simulated data using the theoretical formula of SAXS. For dilute systems where interparticle interactions are negligible (structure factor $S(q) \approx 1$), the scattering intensity $I(q)$ is determined by the product of the particle number density, form factor $P(q,r)$ and particle size distribution. The total scattering intensity is computed as the weighted integral of form factors over all particle sizes, expressed as[27]

$$I(q) \propto \int_{r=0}^{r=r_{\max}} V(r) \cdot P(q,r) \cdot \mathrm{Vol}(r)\,\mathrm{d}r, \tag{1}$$

where $V(r)$ is the distribution of the particle size by volume, q is scattering vector and $\mathrm{Vol}(r)$ is the volume.

For the sphere model, the form factor and volume are given by[27,28]

$$P(q,r) = \left[\frac{3(\sin qr - qr\cdot\cos qr)}{qr^3}\right]^2, \tag{2}$$

$$\mathrm{Vol}(r) = \frac{4}{3}\pi r^3, \tag{3}$$

for the randomly oriented cylinder model, the orientation-averaged form factor was computed via numerical integration over all possible orientations relative to the incident beam:[29,30]

$$P(q,\beta) = 2\int_0^{\pi/2} F^2(q,\beta,r,L)\sin(\beta)\,\mathrm{d}\beta, \tag{4}$$

$$F(q,\beta,r,L) = 2\frac{\sin(\frac{1}{2}qL\cos\beta)}{\frac{1}{2}qL\cos\beta}\frac{J_1(qr\sin\beta)}{qr\sin\beta}, \tag{5}$$

$$\mathrm{Vol}(rL) = \pi r^2 L, \tag{6}$$

where $F(q,\beta)$ is the scattering amplitude of a cylindrical cylinder with different angles β.[31] β is the angle between the scattering vector and cylinder. The L and r represent the length and radius of the cylinder. When employing the cylindrical model to analyze the PSD of solid nanorods, the length distribution is commonly resolved under the premise of a monodisperse radius.

For the randomly oriented ellipsoid model, the form factor is given by[32,33]

$$P(q,R_\mathrm{p},R_\mathrm{e}) = 2\int_0^{\pi/2} F^2(q,\beta,R_\mathrm{p},R_\mathrm{e})\sin(\beta)\,\mathrm{d}\beta, \tag{7}$$

$$F(q,\beta,R_\mathrm{p},R_\mathrm{e}) = \frac{3(\sin qr - qr\cdot\cos qr)}{qr^3}, \tag{8}$$

$$\mathrm{Vol}(R_\mathrm{p},R_\mathrm{e}) = \frac{4}{3}\pi R_\mathrm{p}R_\mathrm{e}^2, \tag{9}$$

where R_p and R_e respectively represent the major axis and the minor axis of the ellipsoid. When conducting PSD calculation based on the ellipsoidal model, it is necessary to preset the size ratio of the major axis to the minor axis of the ellipsoid, which is defined as the aspect ratio. Under the constraint of a fixed aspect ratio $a = R_\mathrm{p}/R_\mathrm{e}$,[31] the PSD estimated by this model is statistically quantified in terms of R_e.

2.2. TSVD-optimized Chahine algorithm

In SAXS experiments, the recorded scattering intensity profile is inherently determined by the structural features of the scattering form model and the statistical distribution of particle sizes within the system. This fundamental relationship between the measured scattering signal and the underlying particulate properties is mathematically known as a Fredholm-type integral equation. Notably, this problem is inherently an ill-posed problem, and its solutions possess non-uniqueness. After discretization, it can be rewritten as a matrix equation in the form

$$I = A \times f, \tag{10}$$

where A is the form factor matrix corresponding to $P(q,r)$ in the formula, reflecting the contribution of particles with different sizes to the scattering intensity. f represents the PSD vector, describing the content proportion of particles with different sizes in the sample, which is to be solved. I is the measured scattering intensity obtained by devices such as photo detectors. The matrix A could be decomposed as follows:

$$A = U\Sigma V^{\mathrm{T}}, \tag{11}$$

where A is a matrix of size $m \times n$ and A has rank r. U is the left singular vector matrix of size $m \times m$. V is the right singular vector matrix of size $n \times n$. Σ is a diagonal matrix of size $m \times n$, containing the singular values of A on its diagonal. The first r singular values in the Σ matrix are non-zero, while the remaining singular values are zero. It can be described in detail as follows:

$$A = [u_1 u_2 \cdots u_m] \begin{bmatrix} \sigma_1 & \cdots & 0 \\ \vdots & \ddots & \vdots \\ 0 & \cdots & \sigma_r \\ \vdots & \cdots & \vdots \\ 0 & \cdots & 0 \end{bmatrix} \begin{bmatrix} v_1^{\mathrm{T}} \\ v_2^{\mathrm{T}} \\ \vdots \\ v_n^{\mathrm{T}} \end{bmatrix}, \tag{12}$$

where the vectors u_1, u_2,..., u_m are the left singular vectors of size $m \times 1$. The vectors v_1, v_2, ..., v_n are the right singular vectors of size $n \times 1$. The scalars σ_1,..., σ_r are the singular values and conventionally listed in decreasing order.[34]

TSVD constructs an approximate matrix by retaining the first k largest singular values and their corresponding singular vectors.[35] The matrix can be written as

$$A \approx A_k = [u_1 u_2 \cdots u_k] \begin{bmatrix} \sigma_1 & \cdots & 0 \\ \vdots & \ddots & \vdots \\ 0 & \cdots & \sigma_k \end{bmatrix} \begin{bmatrix} v_1^{\mathrm{T}} \\ v_2^{\mathrm{T}} \\ \vdots \\ v_k^{\mathrm{T}} \end{bmatrix}. \tag{13}$$

Therefore, the PSD solution of this inverse problem can be expressed as follows:

$$f = \sum_{i=1}^{k} \frac{\left(u_i^{\mathrm{T}} I\right)}{\sigma_i} v_i, \tag{14}$$

only the components corresponding to the first k largest singular values are retained to avoid noise amplification caused by small singular values.

The L-curve method was employed to determine k, leveraging the logarithmic relationship between residual norm and solution norm across candidate truncation orders. This method is effective for ill-posed problems. For each candidate $k \in [1, k_{\max}]$ (where $k_{\max}$ is a user-defined upper bound), two metrics are computed:

$$\mathrm{res_norm}(k) = \left\| A f_k - I \right\|_2, \tag{15}$$

$$\mathrm{sol_norm}(k) = \left\| f_k \right\|_2, \tag{16}$$

where res_norm is residual norm, which quantifies the discrepancy between the predicted and experimental scattering intensities. The sol_norm is solution norm, which measures the solution stability. f_k represents the PSD solution vector obtained by retaining the first k singular values. The first derivative describes how the residual norm changes relative to the solution norm, which is defined as

$$\mathrm{first_deriv}(k) = \frac{\Delta \log(\mathrm{res_norm})}{\Delta \log(\mathrm{sol_norm})}, \tag{17}$$

where $\Delta\log(\mathrm{res_norm})$ and $\Delta\log(\mathrm{sol_norm})$ denote the differences in logarithmic residual norm and solution norm between consecutive truncation orders k and $k+1$, respectively. The second derivative characterizes the rate of change of the first derivative, indicating how the slope of the L-curve evolves with k:

$$\mathrm{second_deriv}(k) = \frac{\Delta \mathrm{first_deriv}}{\Delta \log(\mathrm{sol_norm})}, \tag{18}$$

the L-curve's curvature is computed as

$$\mathrm{curvature}(k) = \frac{|\mathrm{second_deriv}(k)|}{(1 + \mathrm{first_deriv}(k)^2)^{1.5}}, \tag{19}$$

the optimal solution of k is selected by identifying the maximum of the curvature.

When solving for PSD, the Chahine algorithm typically uses a randomly assumed initial value as the starting condition, which often leads to issues of excessive iterations and slow convergence. In this work, using the PSD vector corresponding to the optimal k as the initial condition, the Chahine algorithm is executed to refine the result of PSD through successive iterations that enforce physical constraints (e.g., non-negativity and data consistency). The core principle of the Chahine algorithm is to iteratively modify the PSD of the hypothesis, ensuring that the theoretically reconstructed scattering intensity curve aligns with the experimental scattering intensity curve. The iterative process of PSD can be expressed as

$$f_{j+1}(r) = B_j \odot f_j(r), \tag{20}$$

where j is the number of iterations, r is particle size range, and B_j is an update factor, which is expressed as follows:

$$B_j = \frac{A^{\mathrm{T}} \cdot (I_{\mathrm{EXP}} \oslash (A \cdot f_j))}{\mathrm{sum}(A, \mathrm{dim} = 1)^{\mathrm{T}}}, \tag{21}$$

where $\mathrm{sum}(A, \mathrm{dim} = 1)^{\mathrm{T}}$ is column-wise summation of matrix A, returning a row vector. I_{EXP} is experimental scattering intensity data. Symbol $\oslash$ represents the Hadamard division between two data, which is used to calculate the ratio of the

scattering intensity data from experiment to the j-th iterations results. To ensure the physical plausibility of the inverted results, two critical constraints are enforced at every iteration: the particle-size distribution remains non-negative, and its integral is normalized to unity, guaranteeing both numerical stability and cross-iteration comparability.

3. Functions and performance of GranuSAS

3.1. Functions of GranuSAS

The SAXS data analysis software (GranuSAS) features a user-friendly graphical interface designed for intuitive PSD inversion. The software's functions are divided into three parts: data importation and exportation, inversion computations, and the visualization of results. As shown in Fig. 1, SAXS data can be imported from experimental files or generated synthetically to help users rapidly familiarize themselves with the inversion workflow. When generating SAXS data, users can freely select the particle shape model (sphere, cylinder, or ellipsoid) and specify the size-distribution characteristics to match different material systems. The platform supports mono-, bi-, and tri-modal Gaussian distribution modes, allowing independent assignment of peak position, width, and weight for each mode. In addition, the program features simulation capabilities for Poisson noise (related to fluctuations in x-ray photon counting). By superimposing this type of noise onto the theoretical scattering curve, it can more realistically reproduce the signal characteristics of actual scattering experiments. For PSD inversion, the users only need to set two key parameters — the maximum truncation value and the number of Chahine iterations — before launching the computation. The software employs a parallel architecture that simultaneously inverts the SAXS data using three shape models, while the inversion progress of each model is delivered to the graphical interface in real time. Upon completion, based on the accuracy between each model's scattering data and the input scattering data, the software automatically switches the results interface to the panel of the best-fitting model, providing users with an intuitive recommendation of the best-matched model. Finally, all fitted results are stored for users.

Since the software needs to compute PSD results for three models (spherical, cylindrical, and ellipsoidal), sequential processing of these models would significantly increase the overall processing time. To address this, multi-threaded parallel computing was implemented using the QThread framework. Specifically, the inversion tasks for each model were assigned to independent sub-threads, with each sub-thread performing its respective calculation concurrently in the background. Upon completion of each computational task, the sub-threads transmitted the results to the main thread via the signal-slot mechanism. The main thread then received the results and updated the corresponding content in the software's GUI. Furthermore, to prevent blocking of the main thread during computation, all progress updates were handled asynchronously via the same inter-thread signal-slot mechanism. This ensured that the software interface remained responsive, delivering uninterrupted real-time updates throughout the entire computing process.

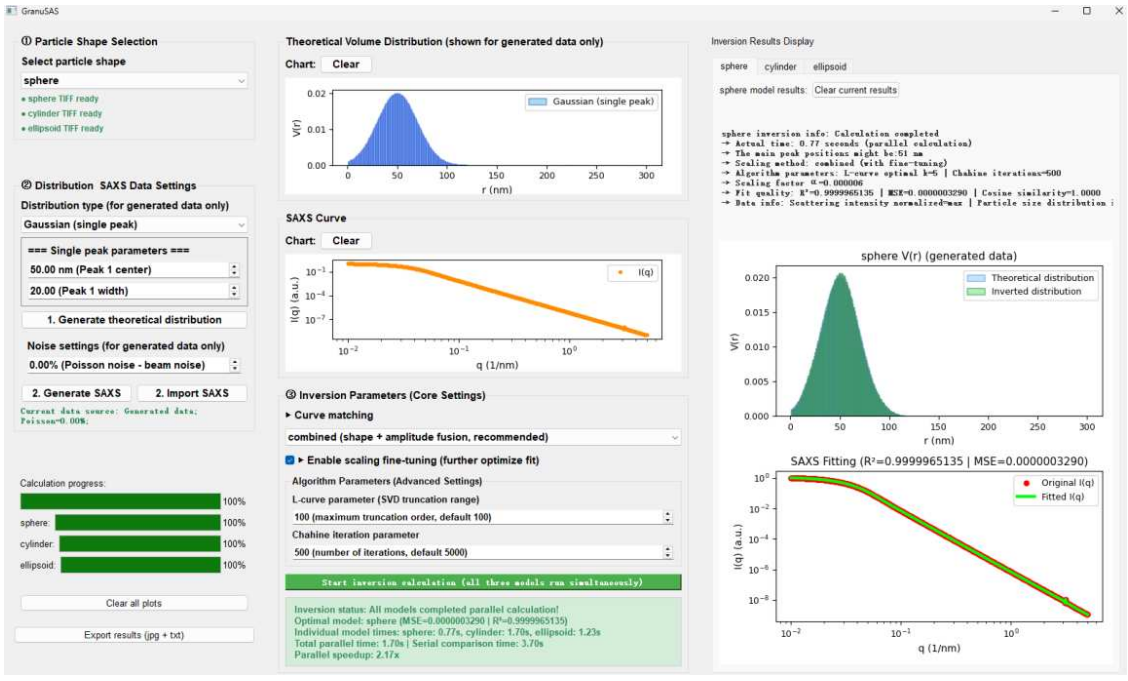


Fig. 1. The main window of the GranuSAS' graphical user interface (GUI) with an example. The GUI is divided into three sections: the left panel for data import and export, the middle panel for TSVD-optimized Chahine algorithm parameters setting and visualization of the input data, and the right panel for visualization of the results.

3.2. Numerical simulation results

In order to verify the performance of GranuSAS, several numerical cases — encompassing mono-, bi-, and trimodal size distributions — were designed for spherical, cylindrical, and ellipsoidal particle models, with a small amount of noise added to the corresponding theoretical scattering curves to approximate experimental conditions. The detailed parameters of each simulated PSD are listed in Table 1. The mathematical expression for the Gaussian peak-type is

$$f(r) = \sum_{1}^{l} w_l \frac{1}{\sigma_l \sqrt{2\pi}} \exp\left(-\frac{(r-\mu_l)^2}{2\sigma_l^2}\right), \tag{22}$$

where r is the radius of the particle, μ_l is the l-th peak position, σ_l is the standard deviation of the l-th peak and w_l is the weight of the l-th peak.

Table 1. Parameters of simulated PSDs data.

Codenamed	Form model	Peak1 (μ_1–σ_1–w_1)	Peak2 (μ_2–σ_2–w_2)	Peak3 (μ_3–σ_3–w_3)
S1	sphere	50–20–1	–	–
S2	sphere	50–20–0.6	180–20–0.4	–
S3	sphere	50–20–0.3	180–20–0.4	250–15–0.3
C1	cylinder	80–15–1	–	–
C2	cylinder	80–15–0.4	180–12–0.6	–
C3	cylinder	80–15–0.3	180–12–0.4	250–15–0.3
E1	ellipsoid	50–5–1	–	–
E2	ellipsoid	50–5–0.6	120–6–0.4	–
E3	ellipsoid	50–5–0.5	120–6–0.4	170–20–0.1

*The radius of the cylinder (C1–C3) is 10 nm, and the aspect ratio of the ellipsoid (E1–E3) is 3.

In order to evaluate the reconstructed results, the coefficient of determination (R^2) and mean square error (MSE) are employed. The formula of R^2 is defined as

$$R^2 = 1 - \frac{\sum_{i=1}^{N} (y_i - \hat{y}_i)^2}{\sum_{i=1}^{N} (y_i - \bar{y})^2}, \tag{23}$$

where y_i is the input data, $\bar{y}$ is the mean value of the input data and $\hat{y}_i$ is the predicted data. An R^2 value nearing 1 signifies an excellent fit of predicted data to the input data, whereas a value approaching 0 indicates a poor fit. Negative R^2 values reflect an anomalous fit, which generally results from model misspecification. The MSE is a commonly used metric to measure the discrepancy between the predicted values and the true values. The formula of MSE is defined as

$$\mathrm{MSE} = \frac{1}{N} \sum_{i=1}^{N} (y_i - \hat{y}_i)^2. \tag{24}$$

A smaller MSE value indicates a higher prediction accuracy.

To demonstrate computational efficiency and accuracy, GranuSAS software was tested against other software, such as McSAS and Irena. McSAS is a commonly used software in SAXS, and we compared it with GranuSAS by analyzing nine simulated scattering datasets (S1–E3). In this study, all software were run on a computer with the following hardware and software configuration: an AMD EPYC 7J13 processor (base frequency of 2.6 GHz, 64 cores, 128 threads), 512 GB of RAM, 1 TB of storage, an NVIDIA GeForce RTX 3060 graphics card, and Windows 10 (64-bit) as the operating system. Leveraging a parallel architecture, GranuSAS simultaneously fits each scattering curve to sphere, cylinder, and ellipsoid models and, upon completion, automatically reports the best-fitting shape. As shown in Table 2, the software-recommended models match the geometries originally used to generate every curve. Beyond this advantage, GranuSAS exhibits superior computational efficiency compared with McSAS. Specifically, for spherical model samples (S1–S3), GranuSAS maintained a stable runtime of 2.86–2.90 s, while McSAS required significantly longer at 9.83–14.6 s — with GranuSAS taking only approximately one-third to one-fifth of McSAS's runtime. The runtime gap between the two software tools widened further in the case of cylindrical model samples (C1–C3). GranuSAS completed the PSD analysis efficiently in 2.14–2.66 s, whereas McSAS's runtime surged to 96.5–442.5 s, showing an order-of-magnitude difference in efficiency. For ellipsoidal model samples (E1–E3), GranuSAS still demonstrated superior efficiency: its runtime ranged from 4.36 s to 6.71 s, while McSAS took 28.05–62 s. Specifically, GranuSAS's runtime was roughly one-fourth to one-ninth that of McSAS.

Table 2. Comparison of calculation times.

Code named	Model suggestions by GranuSAS	Time (s)	
		GranuSAS	McSAS
S1	sphere	2.86	9.83
S2	sphere	2.90	14.07
S3	sphere	2.89	14.6
C1	cylinder	2.18	96.5
C2	cylinder	2.66	316
C3	cylinder	2.14	442.5
E1	ellipsoid	6.71	28.75
E2	ellipsoid	6.61	62
E3	ellipsoid	4.36	28.05

*The fitting parameters for McSAS are as follows: the minimum uncertainty estimate is 5% and the convergence criterion is 1.

Table 3. Comparison of accuracy for reconstructed SAXS data.

Code named	R^2		MSE	
	GranuSAS	McSAS	GranuSAS	McSAS
S1	0.99999925	0.95392903	7.04×10^{-8}	4.32×10^{-3}
S2	0.99999883	0.97600112	4.02×10^{-8}	8.03×10^{-4}
S3	0.99999942	0.96965924	1.5×10^{-8}	7.64×10^{-4}
C1	0.99999938	0.63456193	6.46×10^{-8}	3.819×10^{-2}
C2	0.99999934	0.67353844	5.11×10^{-8}	2.511×10^{-2}
C3	0.99999994	0.64099623	4.1×10^{-9}	2.524×10^{-2}
E1	0.99999995	0.98380362	3.7×10^{-9}	1.28×10^{-3}
E2	0.99999997	0.99881102	2.1×10^{-9}	9.2×10^{-5}
E3	0.99999989	0.97982918	8.3×10^{-9}	1.54×10^{-3}

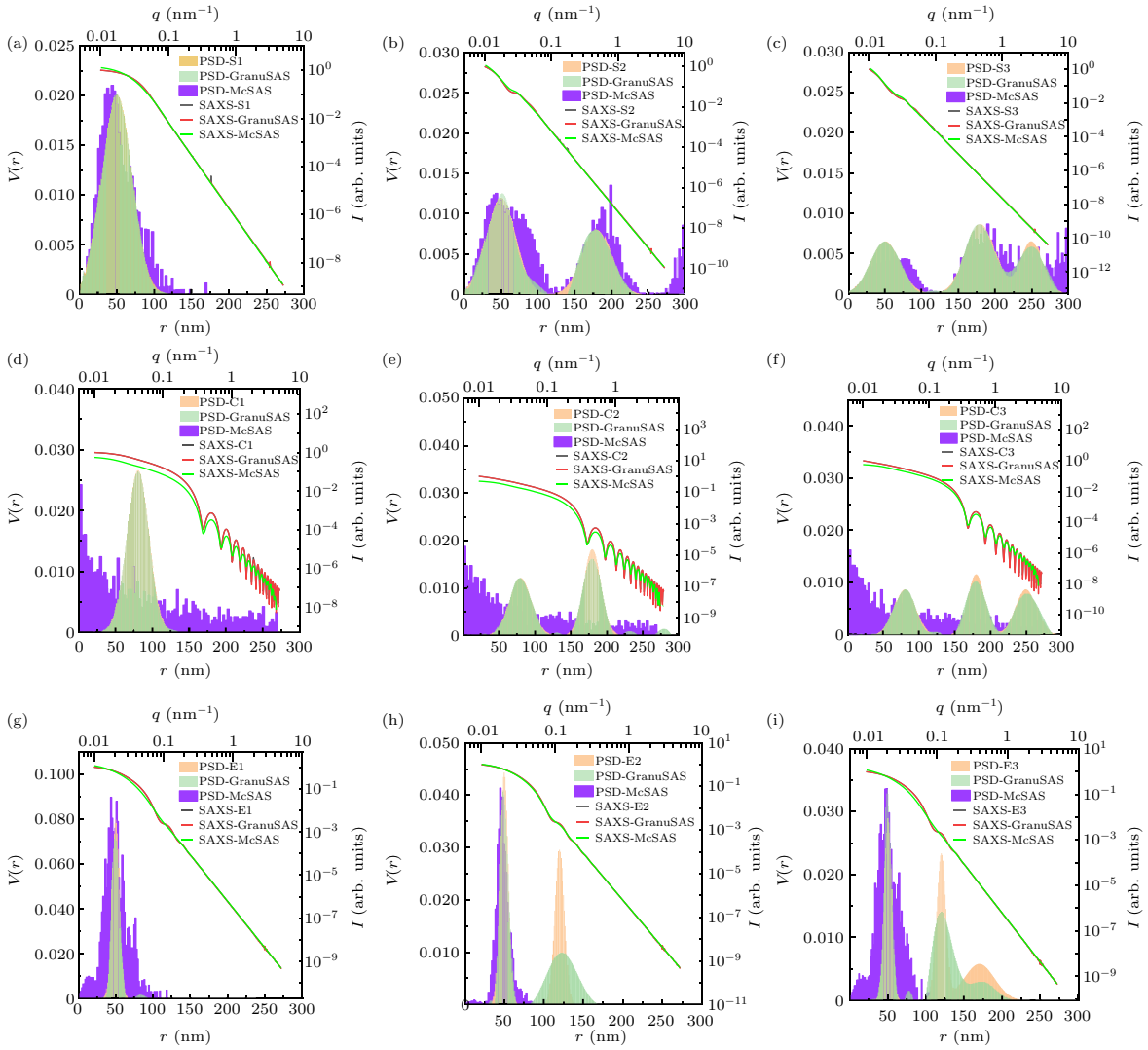


Fig. 2. PSD and scattering curves of simulated and reconstructed data. PSD curves are plotted on the bottom-left axis, with the following color coding: simulated PSD (orange), PSD inverted by GranuSAS (green), and PSD inverted by McSAS (purple). SAXS curves are plotted on the top-right axis, with the following color coding: simulated SAXS curve (black), SAXS curve reconstructed by GranuSAS (red), and SAXS curve reconstructed by McSAS (green). (a)–(c) Spherical models for unimodal, bimodal, and trimodal size distributions, where the bottom abscissa represents the radius of the spheres; (d)–(f) cylinder models for unimodal, bimodal, and trimodal size distributions, where the bottom abscissa represents the half-length of the cylinders; (g)–(h) ellipsoid models for unimodal, bimodal, and trimodal size distributions, where the bottom abscissa represents the minor axis of the ellipsoid.

In terms of the reconstruction of scattering curves, GranuSAS also exhibits a distinct advantage. As shown in Table 3, the R^2 for GranuSAS's reconstructed results is significantly higher than that of McSAS and approaches 1, and MSE of GranuSAS is much smaller than that of McSAS. In addition, figure 2 visually presents all 9 simulated scattering curves and comparatively shows the respective reconstructed SAXS curves of GranuSAS and McSAS. It demonstrates that GranuSAS has superior reconstruction accuracy for SAXS curves. Notably, it can be observed from the results in Table 3 and Fig. 2 that: GranuSAS exhibits excellent reconstruction quality for spherical, cylindrical, and ellipsoidal models; in contrast, McSAS shows differences in its reconstruction performance, it achieves better reconstruction quality for spherical and ellipsoidal models than for cylindrical ones. Subsequently, a comparative analysis was conducted on the PSD results calculated by the two software tools. For the calculation of the S1 and S2 curves, the peak position, peak width, and height obtained by GranuSAS were highly consistent with the theoretical values, as shown in Figs. 2(a) and 2(b). In contrast, there was a certain deviation between the peak position calculated by McSAS and the theoretical PSD. As shown in Fig. 2(c), in the PSD reconstructed by GranuSAS, the peak positions and peak widths of the three characteristic peaks are accurate, but there is a certain discrepancy between the peak proportions and the theoretical PSD. However, the PSD reconstructed by McSAS only exhibits two characteristic peaks, with a significant deviation in the predicted peak position of the first peak. By comparison, in the calculation of the S3 curve, the PSD results calculated by GranuSAS are more consistent with the theoretical PSD. Moving on to the C1–C3 curves, the peak positions and peak widths of the PSD recon-

structed by GranuSAS matched well with the theoretical parameters of PSD as shown in Figs. 2(d)–2(f). However, minor discrepancies were observed in the peak height ratios between the reconstructed bimodal and trimodal distributions and the theoretical values. In stark contrast, the PSD results reconstructed by McSAS showed no match with the theoretical values at all. For the E1 curve, the PSD calculated by GranuSAS was completely consistent with the theoretical PSD. In contrast, the distribution width obtained from McSAS was broader than that of the theoretical PSD, as illustrated in Fig. 2(g). For the E2 curve (see Fig. 2(h)), the positions of the two peaks in GranuSAS's PSD results matched the theoretical PSD. However, the width of the second peak was broader than the theoretical width, and its peak height was lower than the theoretical value. But even worse was that McSAS only yielded a concentrated distribution around the peak position of 50 nm and failed to capture the bimodal distribution characteristic. A similar characteristic was observed for PSD reconstruction of the E3 curve as shown in Fig. 2(i). The GranuSAS again achieved accurate peak position calculations, but slight inconsistencies existed between its predicted second and third peak widths and heights and the theoretical values. Meanwhile, the PSD of McSAS exhibited solely a peak around 50 nm, with no indication of the second or third peaks. Hence, the above results demonstrate that GranuSAS delivers outstanding resolving power for both unimodal and multimodal size distributions. Collectively, GranuSAS significantly surpasses McSAS in computational efficiency and accuracy when analyzing PSDs from simulated scattering curves, which is also further validated by comparing with the Irena software (Figs. S1–S2 and Table S1).

3.3. Experimental results

To systematically verify the performance of the algorithm proposed in this study for nanoparticle characterization, experimental verification studies were carried out. The experimental data were collected at the BL05UB soft x-ray scattering beamline station of the National Synchrotron Radiation Laboratory. In this work, polystyrene nanospheres were selected as experimental samples. Polystyrene nanospheres sample serves as standard material for soft x-ray scattering experiments. Their excellent chemical stability can provide standardized experimental objects for algorithm verification, enabling the evaluation of algorithm accuracy and robustness at the typical nanoscale. The sample for SAXS test is prepared by dropping monodispersed polystyrene solution onto the concave side of a Si_3N_4 window (1.5×1.5 mm^2, 100 nm thickness, 5×5 mm^2 outer frames). Before that, the polystyrene solution was ultrasonicated for 10 min to ensure uniform dispersion. After air drying, weakly attached nanoparticles were removed by gentle air flow to prevent contamination to vacuum chamber. Relying on the synchrotron radiation light source, this beamline station has significant technical advantages such as high photon flux, low divergence angle, and wide energy tuning range. The core technical parameters of the beamline station, including the photon energy range, beam spot size distribution, detector quantum efficiency, etc., are detailed in Table 4.

Table 4. Basic performance parameters of BL05UB.

Optical performance	Result
Light source	EPU50
Energy range	220 eV–700 eV
Resolution power: $E/\Delta E$	1619 @ 244.4 eV
Photon flux	$> 2.74 \times 10^{12}$ phs/s @ 244.4 eV, 360 mA
Beam size	0.375×0.15 mm^2 ($H \times V$)
Detector model	Greateyes Lotte-i 4k4k
Detector pixels	4112×4096
Unit pixel size of detector	15 μm × 15 μm
Detector area	61.68 mm × 61.44 mm

The Greateyes detector was used to record the scattering image, which has the significant advantages of high sensitivity and a wide dynamic range, enabling precise capture of scattering signals with different intensities. During the experiment, the photon energy was set to 410 eV, the exposure time was 10 s, and the sample-to-detector distance was 165 mm. As shown in Fig. 3(a), the two-dimensional image is the collected scatting figure of the detector. The rectangle in the lower right corner of the 2D image is the beam stop, which serves to block the incident x-ray. Figure 3(b) shows the SEM image of polystyrene nanospheres, revealing a radius of approximately 150–160 nm for major particles, along with few larger-diameter and smaller-diameter particles.

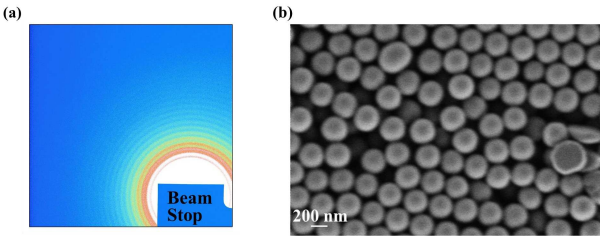


Fig. 3. (a) Two-dimensional experimental SAXS image of polystyrene nanospheres sample, (b) the scanning electron microscope image of polystyrene nanospheres sample.

Then, one-dimensional curves are obtained from the 2D scattering images using ScatterX.[36] For this experimental scattering data, GranuSAS identifies the sphere as the best-fitting shape model, consistent with the actual particle morphology observed in the SEM images. Consequently, the spherical model was likewise adopted for PSD calculation in McSAS. GranuSAS completed the inversion in 1.96 s, whereas McSAS required 30.15 s. This more than fifteen-fold reduction in runtime demonstrates the superior computational efficiency of the GranuSAS software. To verify the accuracy

of the GranuSAS results, this study compared the fitted scattering curves generated by GranuSAS and McSAS (Fig. 4). It is showed that R^2 and MSE between the fitted scattering curve from GranuSAS and the experimental scattering curve reached 0.992683 and 4.295×10^{-4}, respectively; for McSAS, the corresponding R^2 and MSE of its fitted results were 0.983355 and 9.71×10^{-4}, respectively. It can be seen that the goodness of fit of GranuSAS is superior to that of McSAS.

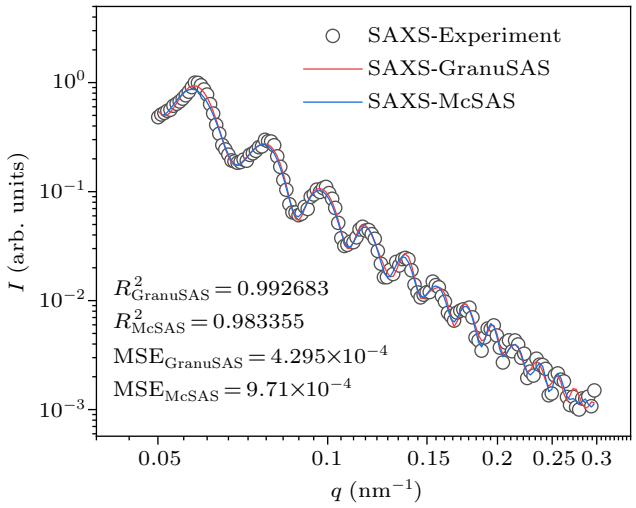


Fig. 4. Comparison of the experimental scattering curve with the scattering curves reconstructed by GranuSAS and McSAS. The experimental scattering curve is derived from the polystyrene nanospheres sample.

Meanwhile, the PSD obtained by statistically analysing SEM images is compared with the PSDs reconstructed from the experimental scattering curve by GranuSAS and McSAS as shown in Fig. 5. It can be seen from the three PSD results that the radii of the vast majority of polystyrene nanoparticles exhibit a concentrated distribution characteristic, with the main distribution range being 150–160 nm. This consistent main distribution range across different characterization approaches confirms the reliability of GranuSAS for the studied system. In addition, the scattering-based inversions reveal minor populations of larger and smaller particles, with their peak positions at approximately 90 nm, 200 nm, and 270 nm, respectively. This finding highlights the high sensitivity of scattering techniques to low-abundance particles, which is beneficial for obtaining a complete understanding of the size distribution in the materials. The direct comparison shows that the PSDs reconstructed by GranuSAS and McSAS are basically consistent with each other, not only in the main distribution range of 150–160 nm but also in the peaks of the minor distribution particle populations. In contrast, the PSD obtained from SEM image statistics fails to capture the full particle size distribution. This comparative analysis not only verifies the consistency and accuracy of PSD results from two independent scattering inversion software (GranuSAS and McSAS) but also explicitly demonstrates the advantage of scattering techniques in terms of statistical representativeness for particulate systems. The advancement of the proposed GranuSAS is also verified by applying RSoXS analysis on the SiO_2 sample with radius around 260 nm (Figs. S3–S5 and Table S2).

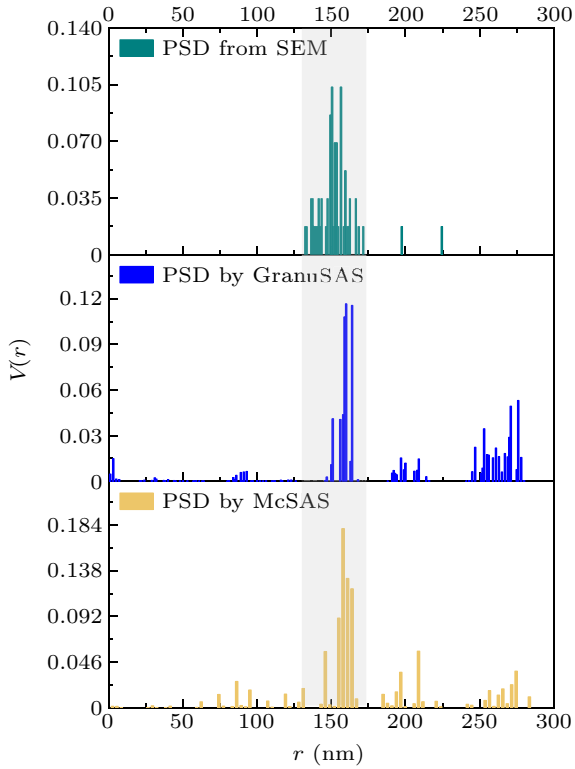


Fig. 5. PSD obtained from statistical analysis of SEM images compared with the PSDs reconstructed by GranuSAS and McSAS.

4. Conclusion

Small angle x-ray scattering (SAXS) has become an important method for analyzing particle size distribution (PSD). In this work, a user-friendly software — GranuSAS — is proposed to the PSD analysis from SAXS data. The software integrates one-click data import/export, simultaneous multi-model inversion, and real-time visualization, enabling non-specialists to conduct high-quality PSD analysis efficiently. Its core algorithm employs the TSVD-optimized Chahine algorithm. Specifically, it determines the optimal truncation parameter through truncated singular value decomposition (TSVD) combined with the *L*-curve method, which effectively suppresses noise interference and addresses the ill-posed nature of the inverse problem. Subsequently, by using the TSVD inversion result as the initial value for the Chahine algorithm, it significantly reduces the number of iterations, thus achieving a balance between computational efficiency and inversion accuracy. The performance of this software is verified via both numerical simulations and experimental data. Compared to the commonly used McSAS software in the field of SAXS, GranuSAS demonstrates several significant advantages. (i) It can perform particle size inversion calculations for spherical, cylindrical, and ellipsoidal models simultaneously, and automatically identify and inform users of the shape model that best matches the input scattering curve based on the inversion

accuracy (e.g., the degree of agreement between the reconstructed scattering curve and the input curve). (ii) It boasts significantly higher computational efficiency, with an operation speed at least three times faster than that of McSAS. (iii) It can deliver accurate inversion results of PSD. (iv) It exhibits high sensitivity in identifying minor peaks in multimodal size distributions. A comparison of the PSD results inverted by GranuSAS and McSAS, and the PSD statistically obtained from the scanning electron microscopy (SEM) image reveals that all three consistently show the main radius of polystyrene nanoparticles is concentrated in the range of 150–160 nm. Among them, the PSD results of GranuSAS and McSAS are highly similar, and this cross-validation result fully confirms the reliability of the inversion results of GranuSAS. In the future, GranuSAS will be further upgraded to expand its functionality: more complex particle shape models (e.g., core–shell structures, irregular polyhedrons) are planned to be integrated. It aims to improve the software's universality for characterizing diverse nanomaterials, thereby providing a powerful tool for the application of SAXS technology in a wider range of materials fields.

Program availability

The source code is openly available in Science Data Bank at https://www.doi.org/10.57760/sciencedb.29272.

Acknowledgments

We thank Hefei Synchrotron Radiation Facility (RSoXS endstation, Jinhua beamline BL05UB, NSRL) for help in the scattering experiments. Project supported by the Project of the Anhui Provincial Natural Science Foundation (Grant No. 2308085MA19), Strategic Priority Research Program of the Chinese Academy of Sciences (Grant No. XDA0410401), the National Natural Science Foundation of China (Grant No. 52202120), the National Key Research and Development Program of China (Grant No. 2023YFA1609800), and USTC Research Funds of the Double First-Class Initiative (Grant No. YD2310002013).

References

[1] Al-Shammari Z, Massoudi I, Rached A, Ababutain I, Alghamdi A I, Algarou N A, Amin K A, Kotb E and Ben Ali A 2025 *Mater. Technol.* **40** 2506674
[2] Caputo F, Clogston J, Calzolai L, Rösslein M and Prina-Mello A 2019 *J. Controlled Release* **299** 31
[3] Indiarto R, Firdaus R G, Marta H, Subroto E, Muhammad D R A and Sikin A M 2025 *Int. J. Food Prop.* **28** 2509992
[4] Xiao C J, Cai W J, Li R D, Ni S, Jiang W T, Wang Z W, Yaqoob K, Chen Z B, Huang Y and Song M 2026 *J. Mater. Sci. Technol.* **242** 1
[5] Gu Q, Zhang H, Liang Z, Li J, Wang Z, Zhou J, Zhong Z, Fan Y and Xing W 2025 *J. Membr. Sci.* **733** 124303
[6] BläUbaum L, Röder F, Nowak C, Chan H S, Kwade A and Krewer U 2020 *ChemElectroChem* **7** 4755
[7] Raj K 2016 *Mater. Powder Rep.* **71** 285
[8] Mostafaei A, De Vecchis P R, Nettleship I and Chmielus M 2019 *Mater. Des.* **162** 375
[9] German R M 1992 *Metall. Trans. A* **23** 1455
[10] Sun J, Wang F, Sui Y, She Z, Zhai W, Wang C and Deng Y 2012 *Int. J. Nanomed.* **7** 5733
[11] Danaei M, Dehghankhold M, Ataei S, Davarani F H, Javanmard R, Dokhani A, Khorasani S and Mozafari M R 2018 *Pharmaceutics* **10** 57
[12] Song Y M, Song L G, Zhu T, Chen Y, Jin S X, Tian F, Hong Z Y, Zhang P, Wang B Y, Wang H H, Yan Q Z, Bian F G and Cao X Z 2021 *J. Nucl. Mater.* **554** 153083
[13] Chokprasombat K, Koyvanich K, Sirisathitkul C, Harding P and Rugmai S 2016 *Trans. Indian Inst. Met.* **69** 733
[14] Larsen A H, Arleth L and Hansen S 2018 *J. Appl. Crystallogr.* **51** 1151
[15] Taché O, Rouzière S, Joly P, Amara M, Fleury B, Thill A, Launois P, Spalla O and Abécassis B 2016 *J. Appl. Crystallogr.* **49** 1624
[16] Zhao H, Wu Z H, Guo M F and Dong B Z 2003 *Chin. Phys. C* **27** 1034
[17] Kyutt R N, Smorgonskaya É A, Danishevskii A M, Gordeev S K and Grechinskaya A V 1999 *Phys. Solid State* **41** 1359
[18] Welborn S S and Detsi E 2020 *Nanoscale Horiz.* **5** 12
[19] Mulato M, Tygel D and Chambouleyron I 1997 *J. Appl. Crystallogr.* **30** 808
[20] Chen R C, Li Z H and He J H 2024 *Nucl. Instrum. Methods Phys. Res. Sect. B-Beam Interact. Mater. Atoms* **552** 165377
[21] Klema V and Laub A 1980 *IEEE Trans. Autom. Control* **25** 164
[22] Hansen P C 1990 *SIAM J. Sci. Stat. Comput.* **11** 503
[23] Grasedyck L 2010 *SIAM J. Matrix Anal. Appl.* **31** 2029
[24] Ferri F, Righini G and Paganini E 1997 *Appl. Opt.* **36** 7539
[25] Tanouye F T, Alves J R, Spinozzi F and Itri R 2023 *Int. J. Biol. Macromol.* **248** 125869
[26] Pauw B R, Pedersen J S, Tardif S, Takata M and Iversen B B 2013 *J. Appl. Crystallogr.* **46** 365
[27] Li Y, Liu L, Zhao X, Zhou S, Wu X, Lai Y, Chen Z, Chen J and Xing X 2024 *Radiat. Detect. Technol. Methods* **8** 1712
[28] Smirnov A V, Deryabin I N and Fedorov B A 2015 *J. Appl. Crystallogr.* **48** 1089
[29] Onsager L 1949 *Ann. N. Y. Acad. Sci.* **51** 627
[30] Feller D, Otten M, Hildebrandt M, Krüsmann M, Bryant G and Karg M 2021 *Soft Matter* **17** 4019
[31] Pedersen J S 1997 *Adv. Colloid Interface Sci.* **70** 171
[32] Isihara A 1950 *J. Chem. Phys.* **18** 1446
[33] Feigin L A and Svergun D I 1987 *Structure analysis by small-angle X-ray and neutron scattering* (Springer New York, NY)
[34] Lange K 2010 *Numerical Analysis for Statisticians* (New York, NY: Springer New York) pp. 129–142
[35] Xu P 1998 *Geophys. J. Int.* **135** 505
[36] Xie M X, Song B Y, Guo Q Y and Jiao X 2024 *Chin. Phys. B* **33** 120101